Synthesis of Diamond Films from Solid Carbon

Randell L. Mills*

Bala Dhandapani

Jiliang He

Jayasree Sankar

BlackLight Power, Inc.
493 Old Trenton Road
Cranbury, NJ 08512

A novel diamond-like carbon film terminated with $CH(1/p)$ (H^*DLC) comprising high binding energy hydride ions was synthesized for the first time from solid carbon by a microwave plasma reaction of a mixture of 10-30% hydrogen and 90-70% helium wherein it is proposed that He^+ served as a catalyst with atomic hydrogen to form the highly stable hydride ions. H^*DLC was identified by time of flight secondary ion mass spectroscopy (ToF-SIMS) and X-ray photoelectron spectroscopy (XPS). TOF-SIMS identified the coatings as hydride by the large H^+ peak in the positive spectrum and the dominant H^- in the negative spectrum. The XPS identification of the H content of the CH coatings as hydride ion $H^-(1/10)$ corresponding to a peak at 49 eV has implications that the mechanism of the diamond-like carbon formation involves one or both of selective etching of graphitic carbon and the activation of surface carbon by the hydrogen catalysis product. Thus, a novel H intermediate formed by the plasma catalysis reaction may serve the role of H, oxygen species, CO, or halogen species used in past systems. Bombardment of the diamond surface by observed, highly energetic species formed by the catalysis reaction may also play a role. By a novel pathway, the relevance of the $C-H-O$ tie line is eliminated along with other stringent conditions and complicated and inefficient techniques which limit broad application of the versatility and superiority of diamond thin film technology.

* Phone: 609-490-1090; Fax: 609-490-1066; E-mail: rmills@blacklightpower.com

I. INTRODUCTION

Diamond has some of the most extreme physical properties of any material such as outstanding mechanical strength, optical transparency, high thermal conductivity, high electron mobility, and unique chemical properties [1]. Thus, a variety of possible applications are envisioned for diamond materials. Yet, its practical use in applications has been limited due to its scarcity, expense, and immalleability. The development of techniques for depositing thin films of synthetic diamonds on a variety of substrates has enabled the exploitation of diamond's superlative properties in many new and exciting applications. These include cutting tools, thermal management of integrated circuits, optical windows, high temperature electronics, surface acoustic wave (SAW) filters, field emission displays, electrochemical sensors, composite reinforcement, microchemical devices and sensors, and particle detectors [1]. But, the fundamental impediment facing the technology at the present is insufficient growth rate of high-quality diamond.

Synthetic diamond was initially commercially produced as single crystals using the so-called high-pressure high-temperature (HPHT) growth technique [1] wherein graphite is compressed in a hydraulic press to tens of thousands of atmospheres, heated to over 2000 K, and left until diamond crystallizes. Recent novel HPHT methods which have been largely unsuccessful, except for the production of nanocrystals by Orwa et. al. [2], are based on attempts to use high energy ion implantation to bury carbon deep in metals or fused silica to take advantage of the large confining pressures there. More versatile thin films have been produced by an addition-of-one-atom-at-a-time approach using chemical vapor deposition (CVD) techniques. All CVD techniques for producing diamond films require activation of the gaseous carbon-containing precursor molecules. To promote diamond over graphite growth, the precursor gas is usually CH_4 that is diluted in excess hydrogen that is typically 99% of the reactant mixture, and the temperature of the substrate is usually maintained in excess of 700°C. Activation may be achieved thermally using a hot filament, gas discharge such as DC, RF, or microwave discharges, or a combustion flame such as an oxyacetylene torch [1].

Although the mechanism of diamond growth on a seed of diamond is still somewhat of a mystery, it is believed to be based on the extraction of H of a CH terminal bond to form a dangling carbon center to which CH_3 reacts. A carbon-carbon bond forms between adjacent methyl groups, and the hydrogen is gradually extracted, probably by H forming H_2. The further preferential degradation of graphitic carbon over diamond carbon by hydrogen permits diamond growth [1]. H may also be required to decrease the concentration of gas phase unsaturated hydrocarbons.

More recent advances of diamond formation have been towards developing methods to grow diamond at low temperatures (< 500°C rather than 700°C) such that diamond films can be grown on a wider range of substrate materials of commercial importance with low melting points such as plastics, aluminum, some glasses, nickel, steel and electronics materials such as *GaAs*. Many gas mixtures have been investigated to achieve this goal including ones containing some halogens, presumably substituting for the role played by H [3]. More common mixtures have different combinations of H_2, CH_4, O_2, CO_2, and CO [3]. Quite successful diamond film growth has been achieved at temperatures as low as 180°C using gas mixtures of CH_4 mixed with CO_2 or CO in microwave plasma deposition reactors wherein an optimal rate is obtained when the gas ratio is about 50/50%. Although the concentration of H_2 in the activated gas mixture is approximately half that seen in the CH_4/ H_2 mixtures [4], the CO_2- CH_4 and CO- CH_4 systems are unique in that hydrogen is low compared to the excess needed in other systems presumably because oxygen species such as O_2, O, and OH in the CO_2- CH_4 and CO- CH_4-system plasmas perform the same role as H in the CH_4- H_2-system plasmas. Recent molecular beam mass spectroscopy investigations of the CO_2- CH_4 system indicate the incorporation of CH_3 at a dangling carbon bond is the most probable mechanism as in the case of the CH_4- H_2 system. However, the species that extracts H may not be an oxygen species. Rather, CO may activate the surface by extracting a terminating H [5].

Empirically it is known that only narrow set of ratios of O, C, and H result in diamond formation. Using the combined data from over 70 diamond deposition experiments, Bachmann et al. produced a $C-H-O$

phase diagram for diamond deposition which showed that low pressure diamond synthesis is only possible within a very narrow well-defined domain centered on a line called the $C-H-O$ tie line [6-7]. A consequence of this analysis was that the exact nature of the plasma gases was unimportant for most CVD processes; rather, the relative ratios of O, C, and H controlled the deposition.

It was previously reported that a novel highly stable surface coating $SiH(1/p)$ which comprised high binding energy hydride ions was synthesized by microwave plasma reaction of mixture of silane, hydrogen, and helium wherein it was proposed that He^+ served as a catalyst with atomic hydrogen to form the highly stable hydride ions [8]. Novel silicon hydride was identified by time of flight secondary ion mass spectroscopy and X-ray photoelectron spectroscopy. The time of flight secondary ion mass spectroscopy (ToF-SIMS) identified the coatings as hydride by the large SiH^+ peak in the positive spectrum and the dominant H^- in the negative spectrum. X-ray photoelectron spectroscopy (XPS) identified the H content of the SiH coatings as hydride ions, $H^-(1/4)$, $H^-(1/9)$, and $H^-(1/11)$ corresponding to peaks at 11, 43, and 55 eV, respectively. The silicon hydride surface was remarkably stable in air for long duration exposure as shown by XPS.

In the quest for low temperature diamond synthesis, CH_4 was substituted for SiH_4 in the helium-hydrogen microwave reaction which formed $SiH(1/p)$. The results are being prepared for submission for publication. In subsequent studies, solid glassy or graphitic carbon was used as the carbon source in the catalytic plasma. We report for the first time the deposition of novel-hydrogen-terminated diamond-like carbon on a silicon-wafer from a solid carbon precursor and a helium-hydrogen (90-70/10-30%) microwave plasma maintained with an Evenson cavity without diamond seeding or abrasion that provides seed crystals [9]. After the plasma processing reaction, the surface was characterized by ToF-SIMS, XPS, and Raman spectroscopy.

II. EXPERIMENTAL

Synthesis

*H*DLC* films were grown on silicon wafer substrates by their exposure to a low pressure *He* / H_2 microwave plasma with 0.1 g of solid glassy carbon foil (0.5 X 0.5 X 0.1 cm, Alpha Aesar 99.99%) or graphite foil (1 X 1 X 0.1 cm, Alpha Aesar 99.99%). The experimental set up comprising a microwave discharge cell operated under flow conditions is shown in Figure 1. The carbon source was placed in the center of the microwave cavity, and a silicon wafer substrate (0.5 X 0.5 X 0.05 cm, Alfa Aesar 99+%) cleaned by heating to 700°C under vacuum was placed about 2 cm off center inside of a quartz tube (1.2 cm in diameter by 25 cm long) with vacuum valves at both ends. The tube was center-fitted with an Opthos coaxial microwave cavity (Evenson cavity) and connected to the gas/vacuum line. The quartz tube and vacuum line were evacuated for 2 hours to remove any trace moisture or oxygen and residual gases. A premixed *He* (90-70%)/H_2 (10-30%) plasma gas was flowed through the quartz tube at a total pressure of 1.5 Torr maintained with a gas flow rate of 40 sccm controlled by a mass flow controller with a readout. The cell pressure was monitored by an absolute pressure gauge. The microwave generator shown in Figure 1 was an Opthos model MPG-4M generator (Frequency: 2450 MHz). The microwave plasma was maintained with a 65 W (forward)/4 W (reflected) power for about 12-16 hrs. The carbon source was located in the center of the plasma, and the substrate was at the cool edge of the plasma glow region. The wall temperature at this position was about 300°C. A thick (~100 μm) translucent, golden-yellow, shiny coating formed on the substrate and the wall of the quartz reactor. The quartz tube was removed and transferred to a drybox with the samples inside by closing the vacuum valves at both ends and detaching the tube from the vacuum/gas line. The coating on the inside of the wall of the reactor tube was collected by etching the tube for 5-10 minutes with 1% dilute hydrofluoric acid. The coating was then detached from the surface and peeled off as a 3 cm long unsupported transparent thin film. The coated silicon wafer substrate was mounted on XPS and ToF-SIMS sample holders under an argon atmosphere in order to prepare samples for the corresponding analyses. Controls for XPS analysis comprised a cleaned commercial silicon wafer (Alfa Aesar 99.99%) and known standards: (a) single crystal diamond, (b) diamond film, (c) glassy carbon, (d) pyrolytic graphite, (e) mineral

graphite, and (f) HDLC (hydrogenated diamond-like carbon). The control for ToF-SIMS analysis comprised a cleaned commercial silicon wafer (Alfa Aesar 99.99%). The coated substrate and thin film were also sent for Raman analysis (Charles Evans & Associates, Sunnyvale, CA).

ToF-SIMS Characterization

A cleaned commercial silicon wafer before and after plasma treatment to form a $H^{*}DLC$ film coating were characterized using a Physical Electronics TRIFT ToF-SIMS instrument. The primary ion source was a pulsed $^{69}Ga^{+}$ liquid metal source operated at 15 keV. The secondary ions were exacted by a ± 3 keV (according to the mode) voltage. Three electrostatic analyzers (Triple-Focusing-Time-of-Flight) deflect them in order to compensate for the initial energy dispersion of ions of the same mass. The 400 pA dc current was pulsed at a 5 kHz repetition rate with a 7 ns pulse width. The analyzed area was $60\mu m$ x $60\mu m$ and the mass range was 0-1000 AMU. The total ion dose was $7X10^{11}\ ions/cm^2$, ensuring static conditions. Charge compensation was performed with a pulsed electron gun operated at 20 eV electron energy. In order to remove surface contaminants and expose a fresh surface for analysis, the samples were sputter-cleaned for 30 s using a $80\mu m$ x $80\mu m$ raster, with 600 pA current, resulting in a total ion dose of $10^{15}\ ions/cm^2$. Three different regions on each sample of $60\mu m$ x $60\mu m$ were analyzed. The positive and negative SIMS spectra were acquired. Representative post sputtering data is reported. The ToF-SIMS data were treated using 'Cadence' software (Physical Electronics), which calculates the mass calibration from well-defined reference peaks.

XPS Characterization

A series of XPS analyses were made on the samples using a Scienta 300 XPS Spectrometer at Lehigh University, Bethlehem, PA. The fixed analyzer transmission mode and the sweep acquisition mode were used. The X-ray incidence angle was 15°. The step energy in the survey scan was $0.5\,eV$, and the step energy in the high resolution scan was $0.15\,eV$. In the survey scan, the time per step was 0.4 seconds, and the number of sweeps was 4. In the high resolution scan, the time per step was 0.3

seconds, and the number of sweeps was 30. $C\,1s$ at $284.5\,eV$ was used as the internal standard.

Raman Spectroscopy

Experimental and control samples were analyzed by Charles Evans & Associates, Sunnyvale, CA. Raman spectra were obtained with a LABRAM spectrometer (Dilor of Jobin Yvon) with a Spectrum One CCD (charge coupled device) detector (Spex and Jobin Yvon) that was air and Peltier cooled. An Omnichrome HeNe laser (Melles Griot) with the light wavelength of 632.817 nm was used as the excitation source. The spectra were taken at ambient conditions and the samples were placed under a Raman microscope (Olympus BX40). Spectra of the film samples were acquired using the following condition: the laser power at the sample was 4 to 8 mW, the slit width of the monochromator was 100 μm which corresponds to a resolution of 3 cm^{-1}, the detector exposure time was 20 mins., and 3 scans were averaged.

III. RESULTS

ToF-SIMS

The positive ion ToF-SIMS spectra ($m/e=0-800$) of a cleaned commercial silicon wafer before and after being coated with a hydrogenated carbon film are shown in Figures 2 and 3, respectively. The positive ion spectrum of the control was dominated by Si^+, oxides $Si_xO_y^+$, and hydroxides $Si_x(OH)_y^+$; whereas, that of the hydrogenated carbon film sample contained no silicon containing fragments. Rather, a large H^+ peak and hydrocarbon fragments $C_xH_y^+$ were observed as given in Table 1.

The negative ion ToF-SIMS spectrum ($m/e=0-800$) of a cleaned commercial silicon wafer before and after being coated with a hydrogenated carbon film are shown in Figures 4 and 5, respectively. The control spectrum was dominated by oxide (O^-) and hydroxide (OH^-); whereas, spectrum of the hydrogenated carbon film was dominated by hydride ion (H^-) and carbon ion (C^-). Very little oxide (O^-) or hydroxide (OH^-) was observed.

XPS

A survey spectrum was obtained over the region $E_b = 0\,eV$ to $1200\,eV$. The primary element peaks allowed for the determination of all of the elements present. The XPS survey scan of a cleaned commercial silicon wafer before and after being coated with a hydrogenated carbon film are shown in Figures 6 and 7, respectively. The major peaks identified in the XPS spectrum of the control sample were $O\,1s$ at 530.6 eV, trace $C\,1s$ at 284.6 eV, dominant $Si\,2s$ at 152.4 eV and $Si\,2p_{3/2}$ at 101.9 eV. Whereas, the hydrogenated carbon film sample comprised only carbon and trace silicon and oxygen contamination as indicated by the trace $O\,1s$ peak at 532.9 eV, the trace $Si\,2s$ at 153.2 eV and $Si\,2p_{3/2}$ at 102.2 eV, and the dominant $C\,1s$ peak at 284.6 eV.

The high resolution XPS spectra (0-35 eV) of the valance band region of (a) single crystal diamond, (b) diamond film, (c) glassy carbon, (d) pyrolytic graphite, (e) mineral graphite, and (f) HDLC are shown in Figure 8 [10]. The corresponding XPS spectrum of the hydrogenated carbon film sample is shown in Figure 9. The film had a broad peak at 16 eV which matched the peak energy of HDLC rather than that of the other forms of carbon which were observed at higher binding energies. An $O\,2s$ peak was also observed at 23 eV as shown in Figure 9.

The high resolution XPS spectra (280-340 eV) of the $C\,1s$ energy loss region of (a) single crystal diamond, (b) diamond film, (c) glassy carbon, (d) pyrolytic graphite, (e) mineral graphite, and (f) HDLC are shown in Figure 10 [10]. The corresponding XPS spectrum of the hydrogenated carbon film sample is shown in Figure 11. Single crystal diamond, diamond film, and HDLC have an energy loss feature which begins at about 290 eV which is at a higher energy than that of the other possible forms of carbon as shown in Figure 10. The closest match to the shape of the energy loss feature of the carbon film is HDLC to which the film was assigned.

The 0-100 eV binding energy region of high resolution XPS spectra of a cleaned commercial silicon wafer before and after being coated with a $H^{*}DLC$ film are shown in Figures 12 and 13 respectively. For comparison, a glassy carbon control spectrum is also shown in Figure 13. The $O\,2s$ peak was observed in each case. In contrast to the glassy carbon and the untreated silicon wafer controls, a novel peak was

observed at 49 eV in the XPS spectrum of the *H*DLC* film. This peak does not correspond to any of the primary elements carbon or oxygen shown in the survey scan in Figure 7, wherein the peaks of these elements are given by Wagner et al. [11]. Hydrogen is the only element which does not have primary element peaks; thus, it is the only candidate to produce the novel peak and correspond to the surface *H* content of the *H*DLC* coatings. This peak closely matched and was assigned to hydride ion $H^-(1/10)$ given previously [12].

Raman

The photomicrograph and the carbon Raman spectrum of the corresponding region of the *H*DLC* film for a first region A are shown in Figures 14 and 15, respectively. The peak positions, full-width-half-maximum (FWHM), and peak areas were calculated by Gaussian curve fitting the baseline corrected spectrum. The diamond peak was observed at 1352.0 cm^{-1}, with a FWHM of 183 cm^{-1}, and the graphite or G-band was observed at 1607.8 cm^{-1} with a FWHM of 92 cm^{-1}. Bands at 520 and 950 cm^{-1} are the first and second order phonons of Si. The band at 2920 cm^{-1} was assigned to an overtone of the G-band.

The carbon Raman spectrum of a second region B of the *H*DLC* film showed the diamond peak at 1302.1 cm^{-1}, with a full-width-half-maximum (FWHM) of 145 cm^{-1}, and the G-band was observed at 1600.3 cm^{-1} with a FWHM of 60 cm^{-1}. The ratio of the areas of the diamond peak to G band, $\frac{I_D}{I_G}$, is considered an indirect measure of carbon $\frac{sp^3}{sp^2}$ bonding ratio. The ratios $\frac{I_D}{I_G}$ for regions A and B were 1.03 and 1.54, respectively. The Raman spectrum confirmed the XPS results that the *H*DLC* film comprised diamond. Raman spectroscopy was also performed on the film from the quartz reactor wall. The results were similar to those of the *H*DLC* film on the silicon substrates. Based on quantitative studies [13-14], we estimate that the diamond composition of the *H*DLC* film was well over 50%.

IV. DISCUSSION

Silicon substrates were coated by the reaction product of a low pressure He (90-70%)/H_2 (10-30%) microwave discharge plasma with glassy or graphitic carbon as the source of C. The ToF-SIMS identified the coatings as hydride by the large H^+ peak in the positive spectrum and the dominant H^- in the negative spectrum. The XPS matched hydrogenated diamond-like carbon, and the H^*DLC films was confirmed to be well over 50% diamond by the intensity of the Raman diamond peak at about 1330 cm^{-1} compared to the G-band at about 1600 cm^{-1}. XPS further identified the surface H content of the H^*DLC coatings as hydride ion $H^-(1/10)$ corresponding to a peak at 49 eV. The novel hydride ion is proposed to form by the catalytic reaction of He^+ with atomic hydrogen and subsequent autocatalytic reactions of $H(1/p)$ to form highly stable carbon hydride products, H^*DLC, comprising $CH(1/p)$ (p is an integer greater than one [12]). The novel highly stable hydride ion formed by the catalytic reaction of He^+ and atomic hydrogen and the energetic reaction itself may be the basis of a novel method of formation of the H^*DLC film from solid carbon. We consider three possible mechanisms based on the unique conditions provided by the catalytic reaction.

In the previously developed CH_4- H_2-system and variations thereof, diamond formation occurs within a small domain about the $C-H-O$ tie line. Stringent conditions of a large excess of hydrogen, diamond seeding, and an elevated temperature are required. Similarly, in the CO_2/ CH_4 system, diamond only formed within a range of a few percent from a 50/50% mixture. We observed for the first time that diamond was very reproducibly formed from a solid carbon source with a helium-hydrogen plasma without the requirements of diamond seeding, an elevated temperature, or an excess of hydrogen, or any particular former set of stringent conditions. Thus, a dramatic breakthrough in thin film diamond deposition has been shown. The presence of novel hydride ions on the surface observed by XPS has implications that the mechanism of diamond-like carbon formation involves one or both of selective etching of graphitic carbon and the activation of surface carbon by the hydrogen catalysis product. Thus, a novel H intermediate formed by the plasma catalysis reaction may serve the role of H, oxygen species, CO, or halogen species used in past systems.

The mechanism may be based on energetic species formed in the plasma reaction. DLC is a metastable material; thus, continuous bombardment of the surface with energetic species that produce thermal and pressure spikes at the growth surface is required for deposition of DLC and related films [15]. By quenching a beam of C^+ ions accelerated in an ultrahigh vacuum to a negatively biased substrate, Aisenberg and Chabot [16] were able to deposit DLC films for the first time. Rather than resulting in commercially useful processes, subsequently developed beam-type and sputtering production methods are essentially used for research. Exemplary methods discussed by Grill and Myerson [17] are single low-energy beams of carbon ions, dual ion beams of carbon and argon, ion plating, RF sputtering or ion-beam sputtering from carbon/graphite targets, vacuum-arc discharges, and laser ablation. Using sputter deposition, amorphous DLC coatings can be prepared at low temperature due to high ion bombardment during the deposition of carbon. The absence of ion bombardment during carbon deposition leads to soft, conductive carbon films with no diamond-like properties. It has been shown that films with more pronounced diamond-like properties are produced at low ion energies (less than 100 eV), and microcrystalline diamond growth, a characteristic feature of DLC films, decreases with increasing ion energy above 100 eV, ultimately giving rise to amorphous graphitic carbon deposition [18-19].

It was reported previously that microwave helium-hydrogen and argon-hydrogen plasmas having catalyst Ar^+ or He^+ showed extraordinary Balmer α line broadening due to hydrogen catalysis corresponding to an average hydrogen atom temperature of $110\text{-}130\,eV$ and $180\text{-}210\,eV$, respectively; whereas, plasmas of pure hydrogen, neon-hydrogen, krypton-hydrogen, and xenon-hydrogen showed no excessive broadening corresponding to an average hydrogen atom temperature of $\approx 3\,eV$ [20-22] Thus, the energetic species such as fast H formed in the helium-hydrogen microwave plasma may be the basis of the formation of the H^*DLC film from solid carbon. The results of the formation of diamond films by vapor deposition of carbon in the presence of an argon-hydrogen plasma wherein Ar^+ serves as a catalyst are being prepared for submission for publication.

Alternatively, the binding of novel H to graphitic carbon may cause a conversion to the diamond form. Novel EUV emission lines from microwave and glow discharges of helium with 2% hydrogen with energies of $q \cdot 13.6\, eV$ where $q = 1,2,3,4,6,7,8,9,11,12$ or these lines inelastically scattered by helium atoms in the excitation of $He\,(1s^2)$ to $He\,(1s^1 2p^1)$ were identified as novel H intermediates [21]. And, novel hydride compounds MH^* and MH_2^* wherein M is the alkali or alkaline earth metal and H^* comprising a novel high binding energy hydride ions were identified previously [23-25] by a large distinct upfield resonance that showed that the hydride ion was different from the hydride ion of the corresponding known compound of the same composition [23]. Pronounced effects of dopants on the structure and properties of crystalline materials is well known [26-27]. In the case of carbon, the binding of the novel H may thermodynamically favor the diamond form of carbon over the graphitic form which could be the basis of the mechanism for the formation of diamond under our unique conditions.

It has been shown that solid carbon can be converted to diamond, using a catalytic plasma reaction. Large scale production of diamond films under relatively mild, robust conditions is anticipated.

ACKNOWLEDGMENTS

Thanks to P. Ray for useful discussions, to A. Miller of Lehigh University for XPS analysis and very useful discussions, and V. Pajcini of Charles Evans & Associates for Raman analysis and useful discussions.

REFERENCES

1. P. W. May, "Diamond thin films: a 21 st-century material", Phil. Trans. R. Soc. Lond. A, Vol. 358, (2000), pp. 473-495.
2. J. O. Orwa, S. Prawer, D. N. Jamieson, J. L. Peng, J. C. McCallum, K. W. Nugent, Y. J. Li, L. A. Bursill, "Diamond nanocrystals formed by direct implantation of fused silica with carbon", Journal of Applied Physics, Vol. 90, No. 6, (2001), pp. 3007-3018.
3. M. A. Elliott, P. W. May, J. Petherbridge, S. M. Leeds, M. N. R. Ashfold, W. N. Wang, "Optical emission spectroscopic studies of microwave

enhanced diamond CVD using CH_4/CO_2 plasmas", Diamond and Related Materials, Vol. 9, (2000), pp. 311-316.

4. J. R. Petherbridge, P. W. May, S. R. J. Pearce, K. N. Rosser, M. N. R. Ashfold, "Low temperature diamond growth using CO_2/CH_4 plasmas: Molecular beam mass spectroscopy and computer simulation investigations", Journal of applied Physics, Vol. 89, No. 2, Jan. 15, (2001), pp. 1484-1492.
5. J. Petherbridge, P. W. may, S. R. J. Pearce, K. N. Rosser, M. N. R. Ashfold, "Molecular beam mass spectrometry investigations of low temperature diamond growth using CO_2/CH_4 plasmas", Diamond and Related Materials, Vol. 10, (2001), pp. 393-398.
6. P. K. Bachmann, D. Leers, H. Lydtin, D. U. Wiechert, Diamond and Related Materials, Vol. 1, No. 1, (1991), p. 1.
7. P. K. Bachmann, H. G. Hagemann, H. Lade, D. Leers, F. Picht, D. U. Wiechert, Mater. Res. Soc. Proc., Vol. 339, (1994), p. 267.
8. R. L. Mills, B. Dhandapani, J. He, "Synthesis and Characterization of a Highly Stable Amorphous Silicon Hydride", Int. J. Hydrogen Energy, submitted.
9. J. H. D. Rebello, D. L. Straub, V. V. Subramaniam, "diamond growth from a CO/CH_4 mixture by laser excitation of CO: Laser excited chemical vapor deposition", J. Appl. Phys., Vol. 72, No. 3, (1992), pp. 133-1136.
10. Provided by A. Miller, Zettlemoyer Center for Surface Studies, Sinclair Laboratory, Lehigh University Bethlehem, PA.
11. 45. C. D. Wagner, W. M. Riggs, L. E. Davis, J. F. Moulder, G. E. Mulilenberg (Editor), *Handbook of X-ray Photoelectron Spectroscopy*, Perkin-Elmer Corp., Eden Prairie, Minnesota, (1997).
12. R. Mills, *The Grand Unified Theory of Classical Quantum Mechanics*, September 2001 Edition, BlackLight Power, Inc., Cranbury, New Jersey, Distributed by Amazon.com; posted at www.blacklightpower.com.
13. S. M. Leeds, T. J. Davis, P. W. May, C. D. O. Pickard, M. N. R. Ashfold, "Use of different wavelengths for analysis of CVD diamond by laser Raman Spectroscopy", Diamond and Related Materials, Vol. 7, (1998), pp. 233-237.
14. K. W. R. Gilkes, S. Prawer, K. W. Nugent, J. Robertson, H. S. Sands, Y. Lifshitz, X. Shi, "Direct quantitative detection of the sp^3 bonding in diamond-like carbon films using ultraviolet and visible Raman

spectroscopy", Journal of Applied Physics, Vol. 87, No. 10, (2000), pp. 7283-7289.
15. C. Weissmantel, *Thin Films from Free Atoms and Molecules*, K. J. Klabunde, Ed., Academic Press, Inc., New York, (1985), p. 153.
16. S. Aisenberg, R. Chabot, J. Appl. Phys., Vol. 42, (1971), p. 2953.
17. A. Grill, B. Meyerson, *Synthetic Diamond: Emerging CVD Science and Technology*, K. E. Spear and J. P. Dismukes, Eds., John Wiley & Sons, Inc., New York, (1994), p. 91.
18. J. Ishikawa, K. Ogawa, K. Miyata, T. Takagi, Nucl. Instrum. Methods, Vol. B21, (1987), p. 205.
19. F. Rossi, B. Andre, in Proc. IP AT 1991, Brussels, CEP Consultants, Edinburgh, UK, (1991), p. 43.
20. R. L. Mills, P. Ray, B. Dhandapani, J. He, "Comparison of Excessive Balmer α Line Broadening of Glow Discharge and Microwave Hydrogen Plasmas with Certain Catalysts", J. of Applied Physics, submitted.
21. R. L. Mills, P. Ray, B. Dhandapani, M. Nansteel, X. Chen, J. He, "New Power Source from Fractional Rydberg States of Atomic Hydrogen", Chem. Phys. Letts., in press.
22. R. L. Mills, P. Ray, "Substantial Changes in the Characteristics of a Microwave Plasma Due to Combining Argon and Hydrogen", New Journal of Physics, www.njp.org, Vol. 4, (2002), pp. 22.1-22.17.
23. R. Mills, B. Dhandapani, M. Nansteel, J. He, A. "Voigt, Identification of Compounds Containing Novel Hydride Ions by Nuclear Magnetic Resonance Spectroscopy", Int. J. Hydrogen Energy, Vol. 26, No. 9, Sept. (2001), pp. 965-979.
24. R. Mills, B. Dhandapani, N. Greenig, J. He, "Synthesis and Characterization of Potassium Iodo Hydride", Int. J. of Hydrogen Energy, Vol. 25, Issue 12, December, (2000), pp. 1185-1203.
25. R. Mills, B. Dhandapani, M. Nansteel, J. He, T. Shannon, A. Echezuria, "Synthesis and Characterization of Novel Hydride Compounds", Int. J. of Hydrogen Energy, Vol. 26, No. 4, (2001), pp. 339-367.
26. K. Kim, G. Hong, D. Won, B. Kim, H. Moon, D. Suhr, "Microstructure, microhardness, and superconductivity of CeO_2-added $Y-Ba-Cu-O$ superconductors", J. Mater. Res., Vol. 7, No. 9, p.2349.
27. M. C. Martin, G. Shirane, Y. Endoh, K. Hirota, Y. Moritomo, Y. Tokura, "Magnetism and structural distortion in the $La_{0.7}Sr_{0.3}MnO_3$ metallic

ferromagnet", Physical Review B, Vol. 53, No. 21, (1996), pp. 14,285-14,290.

Table 1. Positive ToF-SIMS fragments of the hydrogenated carbon film formed on a silicon substrate from a helium-hydrogen (95/5%) microwave plasma with the glassy carbon as the souce of *C*. The mass was calibrated by *H* (1.0078) and C_2H_3 (27.0235).

M/Z	Fragment / Ion (+) (Count Integral > 500)	M/Z	Fragment / Ion (+) (200 < Count Integral <500)
1.0078	H	28.0310	C_2H_4
12.0000	C	30.9997	H_3Si
13.0078	CH	40.0291	C_3H_4
14.0157	CH_2	42.0441	C_3H_6
15.0246	CH_3	50.0088	C_4H_2
26.0150	C_2H_2	51.0218	C_4H_3
27.0238	C_2H_3	65.0370	C_5H_5
29.0405	C_2H_5	67.0565	C_5H_7
39.0229	C_3H_3	77.0297	C_6H_5
41.0404	C_3H_5	79.0386	C_6H_7
43.0576	C_3H_7	81.0722	C_6H_9
53.0390	C_4H_5	83.0968	C_6H_{11}
55.0567	C_4H_7	85.1123	C_6H_{13}
57.0739	C_4H_9	91.0494	C_7H_7
69.0719	C_5H_9	93.0653	C_7H_9
71.0929	C_5H_{11}	95.0893	C_7H_{11}
73.0751	C_4H_9O	97.1010	C_7H_{13}
		113.0926	$C_7H_{13}O$
		147.0965	$C_{10}H_{11}O$

Figure Captions

Figure 1. The experimental set up comprising a microwave discharge cell operated under flow conditions.

Figure 2. The positive ion ToF-SIMS spectra ($m/e = 0-800$) of a noncoated cleaned commercial silicon wafer (Alfa Aesar 99.9%).

Figure 3. The positive ion ToF-SIMS spectra ($m/e = 0-800$) of a cleaned commercial silicon wafer (Alfa Aesar 99.9%) coated with a hydrogenated carbon film that showed a large H^+ peak and hydrocarbon fragments $C_xH_y^+$ given in Table 1.

Figure 4. The negative ion ToF-SIMS spectrum ($m/e = 0-800$) of a noncoated cleaned commercial silicon wafer (Alfa Aesar 99.99%).

Figure 5. The negative ion ToF-SIMS spectrum ($m/e = 0-800$) of a cleaned commercial silicon wafer (Alfa Aesar 99.9%) coated with a hydrogenated carbon film that was dominated by hydride ion.

Figure 6. The XPS survey scan of a cleaned commercial silicon wafer (Alfa Aesar 99.9%). Only silicon, oxygen, and trace carbon contamination were observed.

Figure 7. The XPS survey scan of a cleaned commercial silicon wafer (Alfa Aesar 99.9%) coated by reaction of a helium-hydrogen plasma with solid glassy carbon as the source of *C*. Only carbon and trace silicon and oxygen contamination were observed.

Figure 8. High resolution XPS spectra (0-35 eV) of the valance band region of (a) single crystal diamond, (b) diamond film, (c) glassy carbon, (d) pyrolytic graphite, (e) mineral graphite, and (f) HDLC.

Figure 9. High resolution XPS spectra (0-35 eV) of the valance band region of a cleaned commercial silicon wafer (Alfa Aesar 99.9%) coated with a hydrogenated carbon film that showed features that matched HDLC. An *O* 2*s* peak was also observed at 23 eV.

Figure 10. High resolution XPS spectra (280-340 eV) of the *C* 1*s* energy loss region of (a) single crystal diamond, (b) diamond film, (c) glassy carbon, (d) pyrolytic graphite, (e) mineral graphite, and (f) HDLC.

Figure 11. High resolution XPS spectrum (280-340 eV) of the *C* 1*s* energy loss region of a cleaned commercial silicon wafer (Alfa Aesar 99.9%) coated with a hydrogenated carbon film that showed features that matched HDLC.

Figure 12. The 0-100 eV binding energy region of a high resolution XPS spectrum of a cleaned commercial silicon wafer showing only a large $O\,2s$ peak in the low binding energy region.

Figure 13. The overlay of the 0-100 eV binding energy region of a high resolution XPS spectrum of glassy carbon and a cleaned commercial silicon wafer coated with a $H^{*}DLC$ film. A novel peak observed at 49 eV which could not be assigned to the elements identified by their primary XPS peaks matched and was assigned to $H^{-}(1/10)$. The novel highly stable hydride ion formed by the catalytic reaction of He^{+} and atomic hydrogen may be the basis of the novel method of formation of the $H^{*}DLC$ film.

Figure 14. The photomicrograph of a first region A of a $H^{*}DLC$ film on a silicon wafer that was analyzed by Raman spectroscopy.

Figure 15. The Raman spectrum recorded on region A shown in Figure 14. The diamond peak and G band were observed at 1352.0 cm^{-1} and 1607.8 cm^{-1}, respectively.

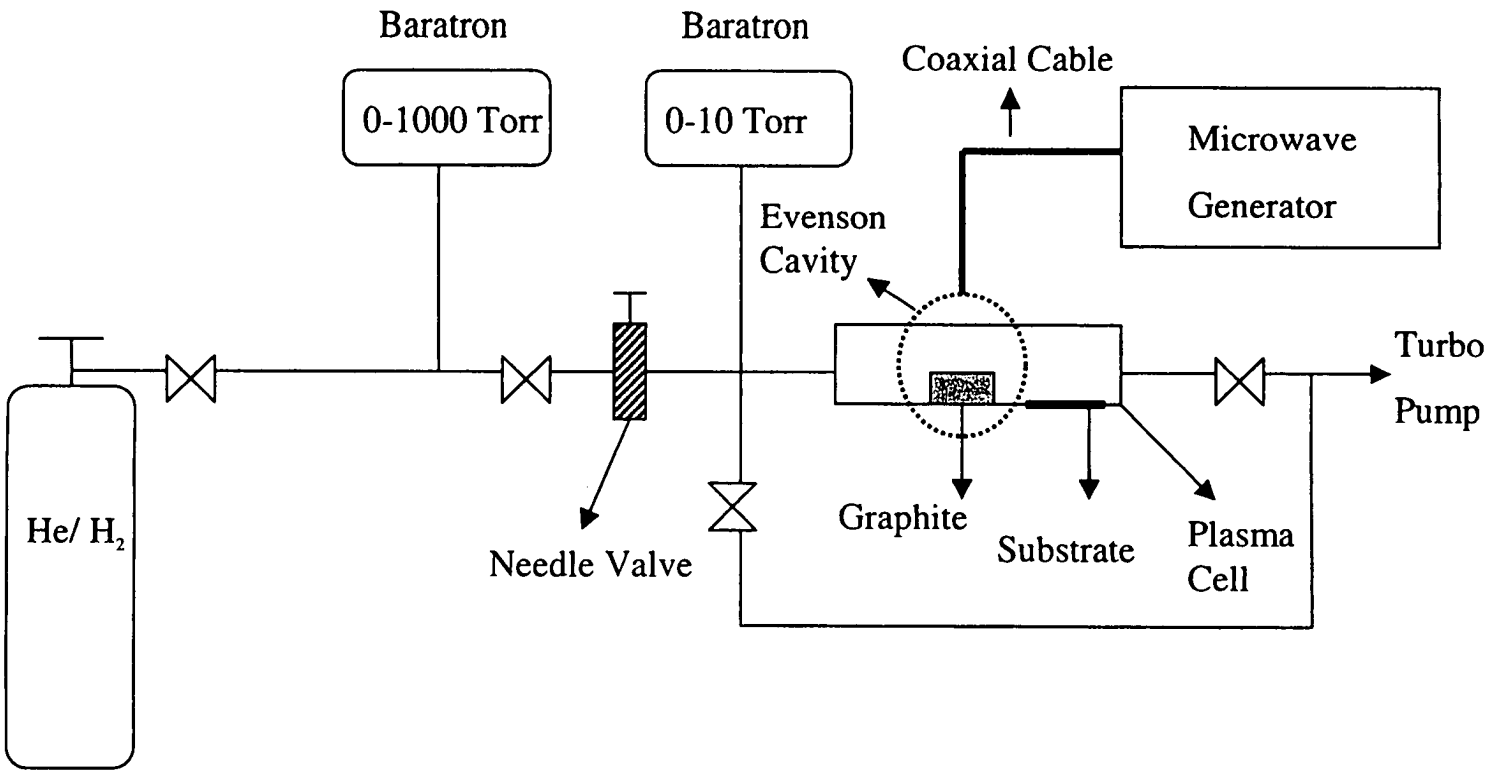
Baratron
0-1000 Torr
Baratron
0-10 Torr
Coaxial Cable
Microwave
Generator
Evenson
Cavity
Turbo
Pump
He/ H_2
Needle Valve
Graphite
Substrate
Plasma
Cell

Fig. 1

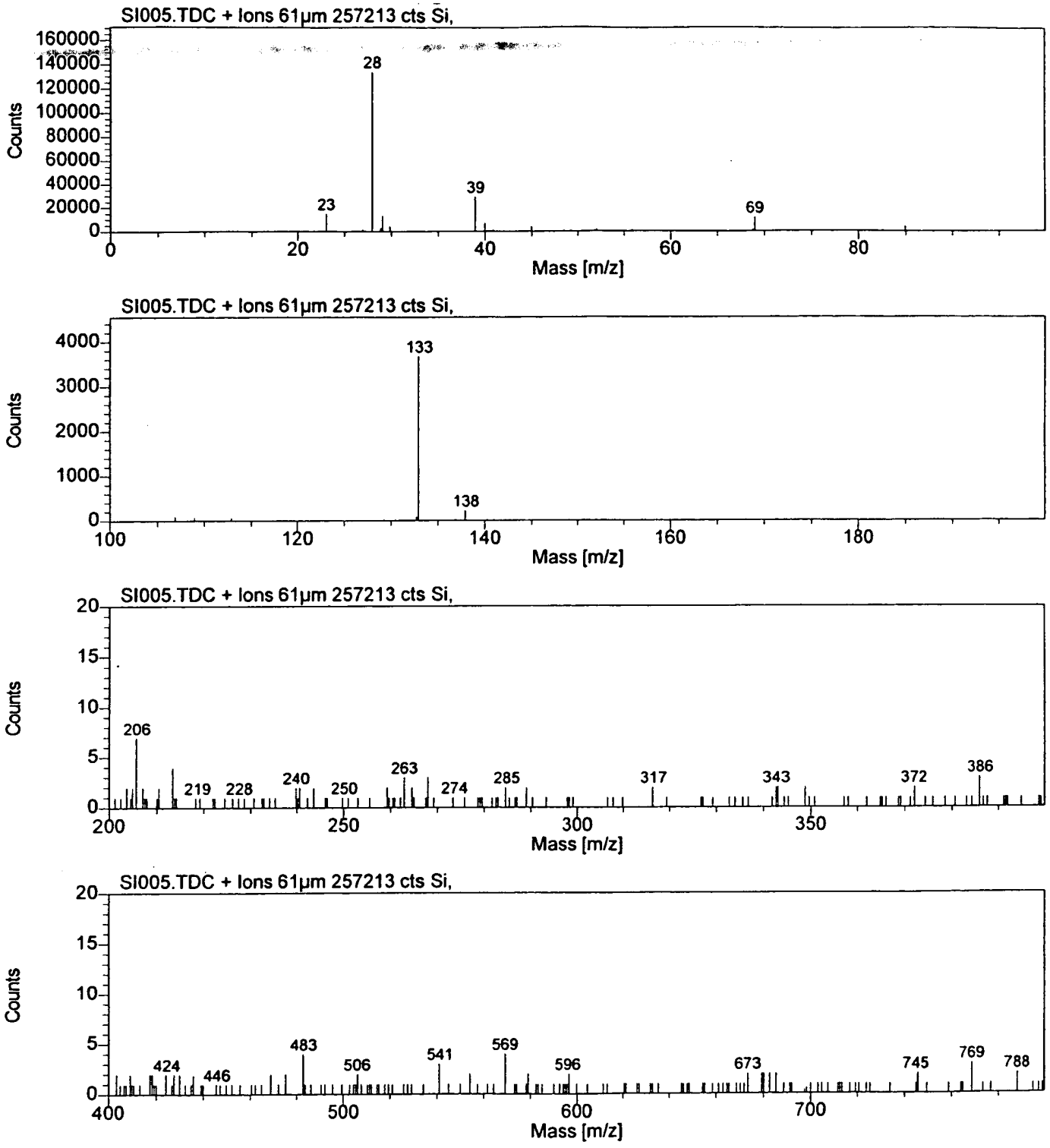
SI005.TDC + Ions 61µm 257213 cts Si,
Counts
Mass [m/z]
28
23
39
69
133
138
206
219
228
240
250
263
274
285
317
343
372
386
483
424
446
506
541
569
596
673
745
769
788

Fig. 2

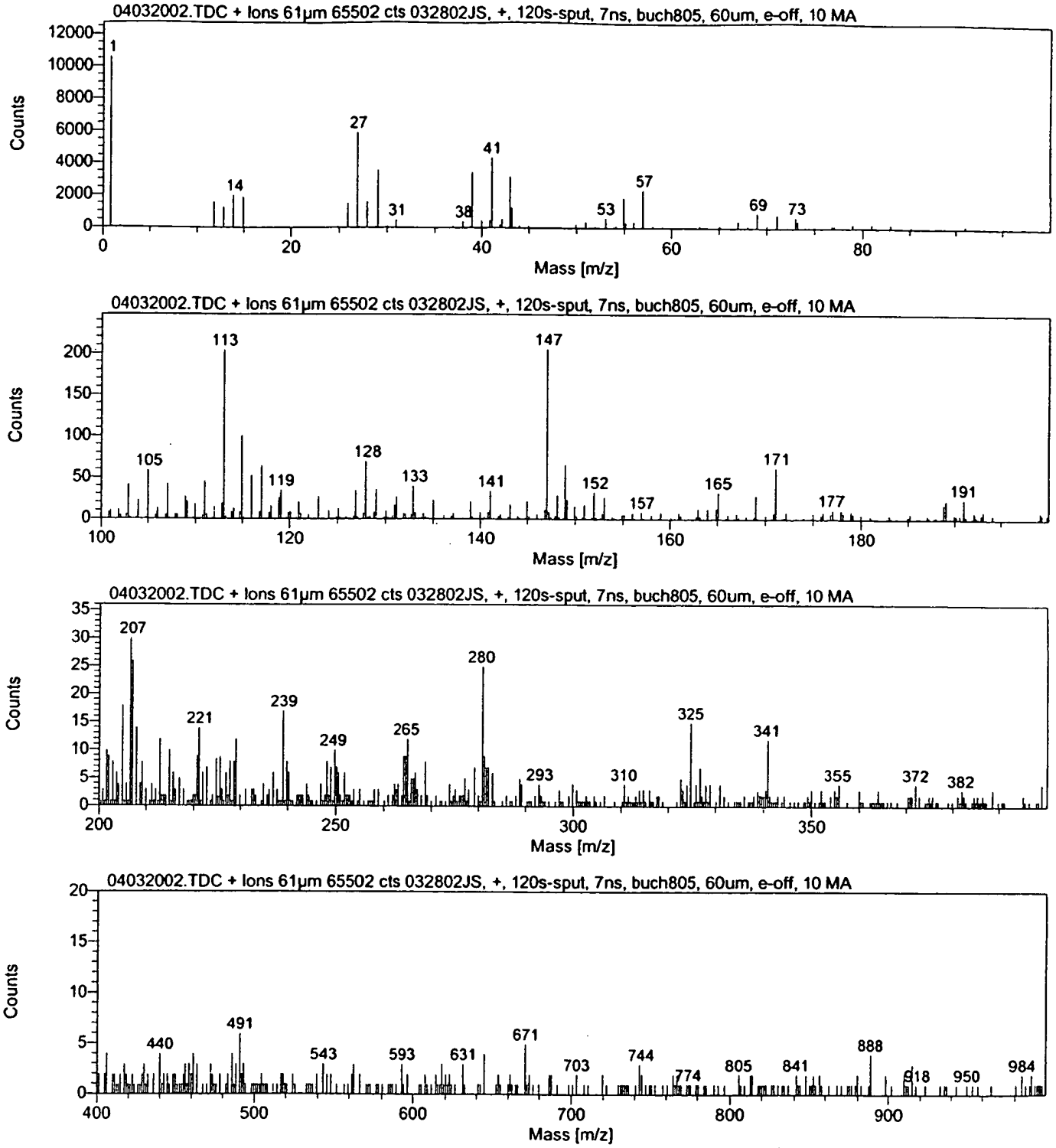
04032002.TDC + Ions 61µm 65502 cts 032802JS, +, 120s-sput, 7ns, buch805, 60um, e-off, 10 MA
Counts
Mass [m/z]
1
14
27
31
38
41
53
57
69
73
113
105
119
128
133
141
147
152
157
165
171
177
191
207
221
239
249
265
280
293
310
325
341
355
372
382
440
491
543
593
631
671
703
744
774
805
841
888
918
950
984

Fig. 3

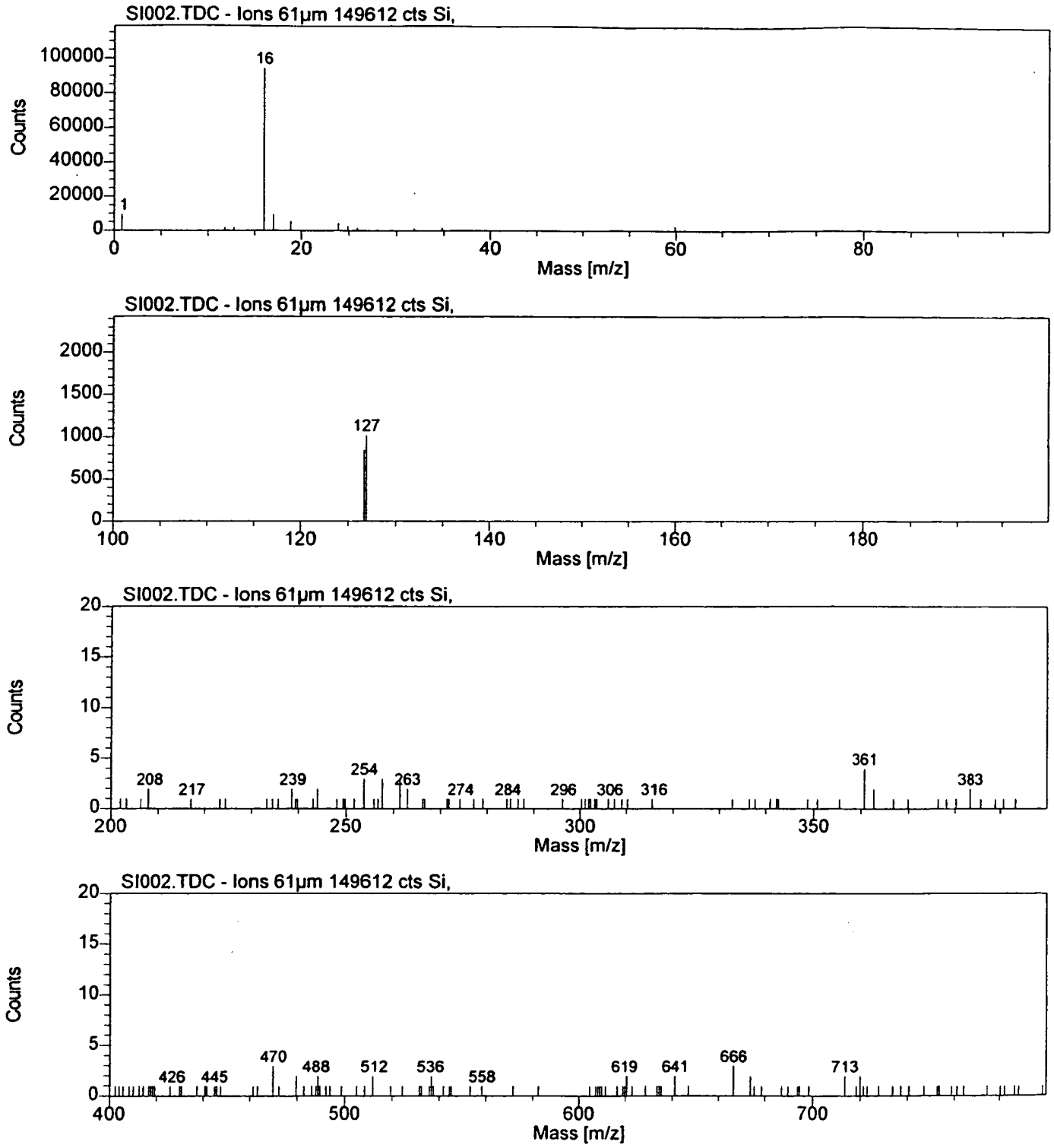
SI002.TDC - Ions 61µm 149612 cts Si,
Counts
Mass [m/z]
16
1
SI002.TDC - Ions 61µm 149612 cts Si,
127
SI002.TDC - Ions 61µm 149612 cts Si,
208
217
239
254
263
274
284
296
306
316
361
383
SI002.TDC - Ions 61µm 149612 cts Si,
426
445
470
488
512
536
558
619
641
666
713

Fig. 4

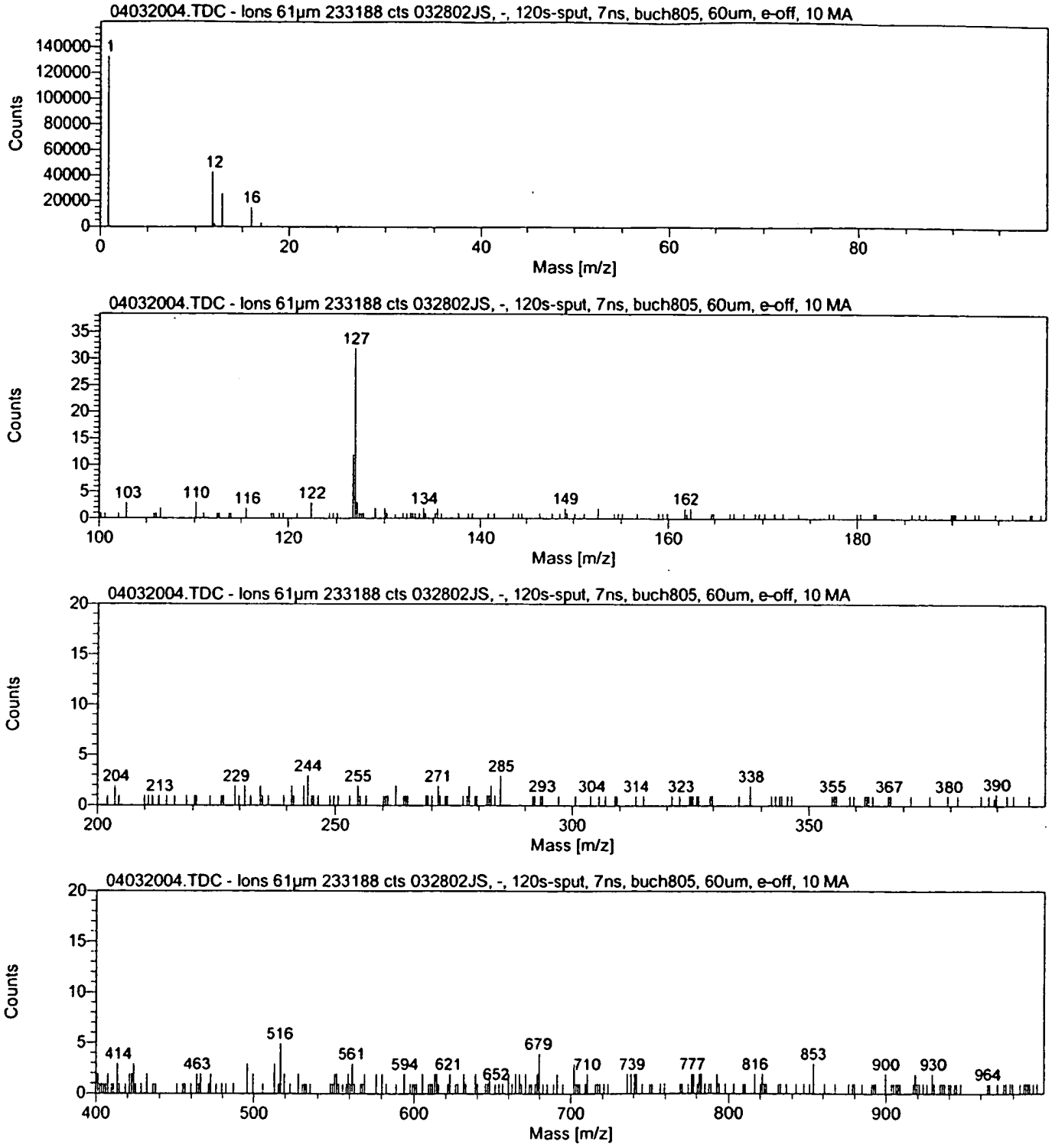
04032004.TDC - Ions 61µm 233188 cts 032802JS, -, 120s-sput, 7ns, buch805, 60um, e-off, 10 MA
Counts
Mass [m/z]
1
12
16
127
103
110
116
122
134
149
162
204
213
229
244
255
271
285
293
304
314
323
338
355
367
380
390
414
463
516
561
594
621
652
679
710
739
777
816
853
900
930
964

Fig. 5

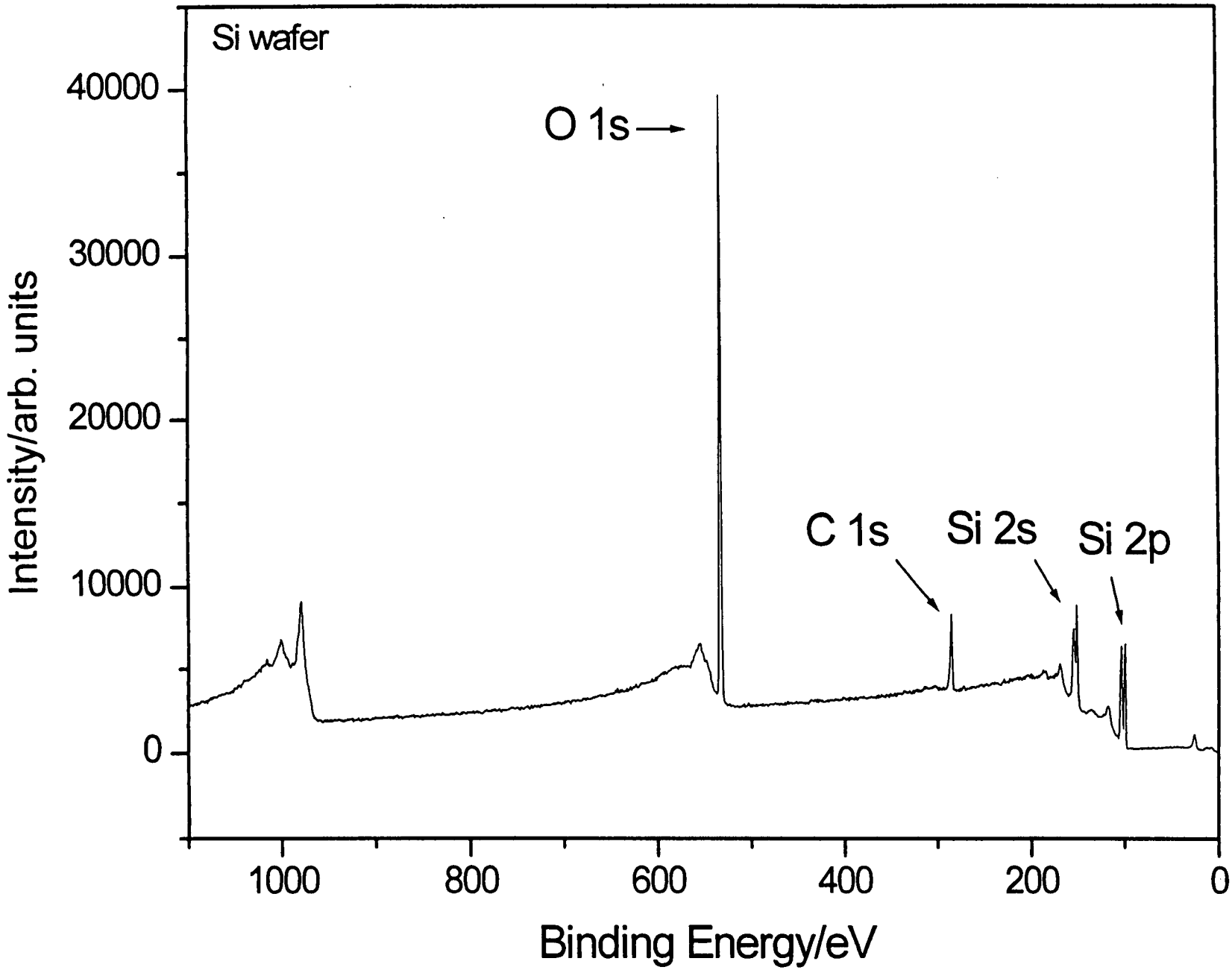
Si wafer
O 1s
C 1s
Si 2s
Si 2p
40000
30000
20000
10000
0
Intensity/arb. units
1000
800
600
400
200
0
Binding Energy/eV

Fig. 6

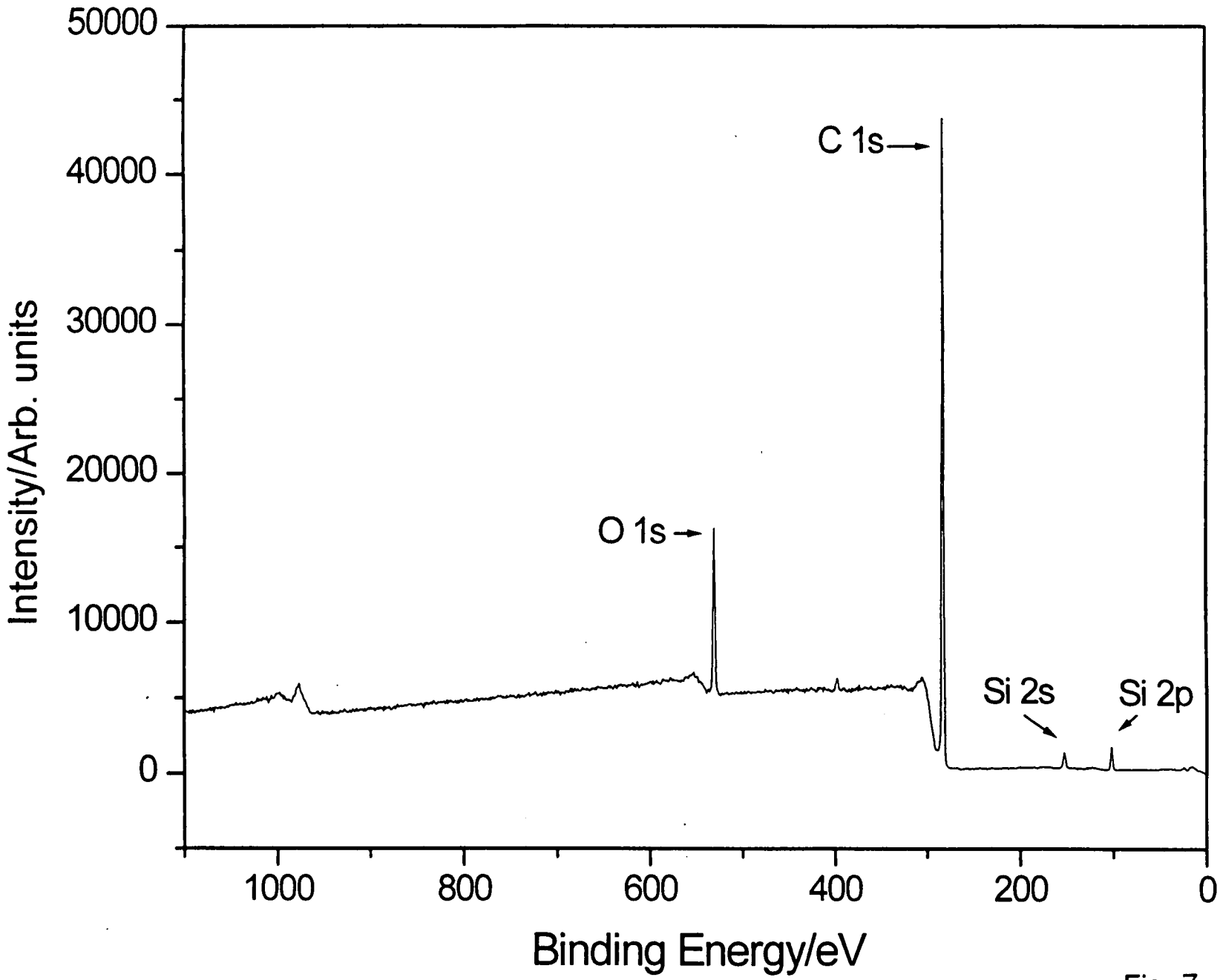
sample: 021802JS
50000
40000
30000
20000
10000
0
Intensity/Arb. units
C 1s
O 1s
Si 2s
Si 2p
1000
800
600
400
200
0
Binding Energy/eV

Fig. 7

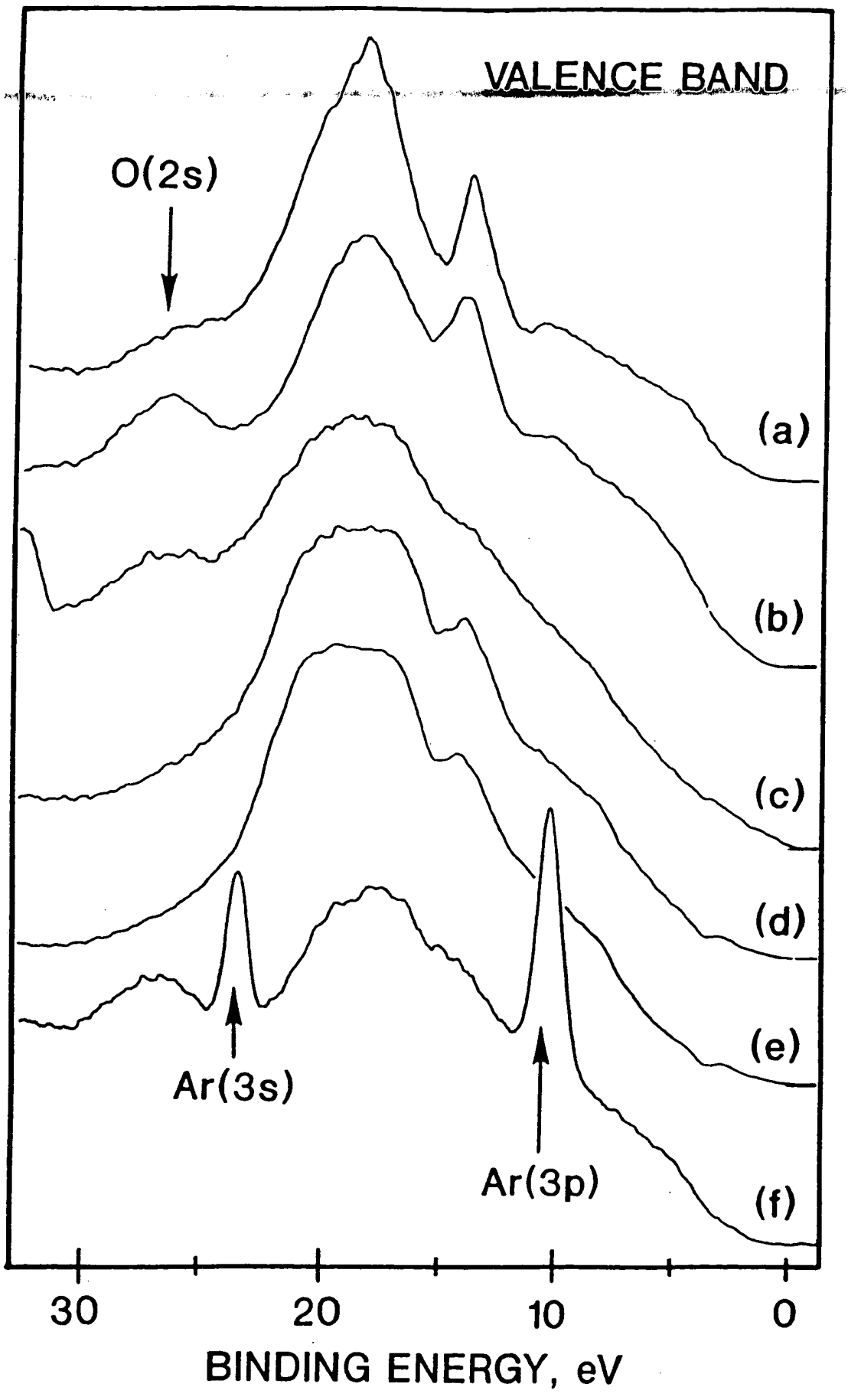
VALENCE BAND
O(2s)
(a)
(b)
(c)
(d)
(e)
(f)
Ar(3s)
Ar(3p)
30
20
10
0
BINDING ENERGY, eV

Fig. 8

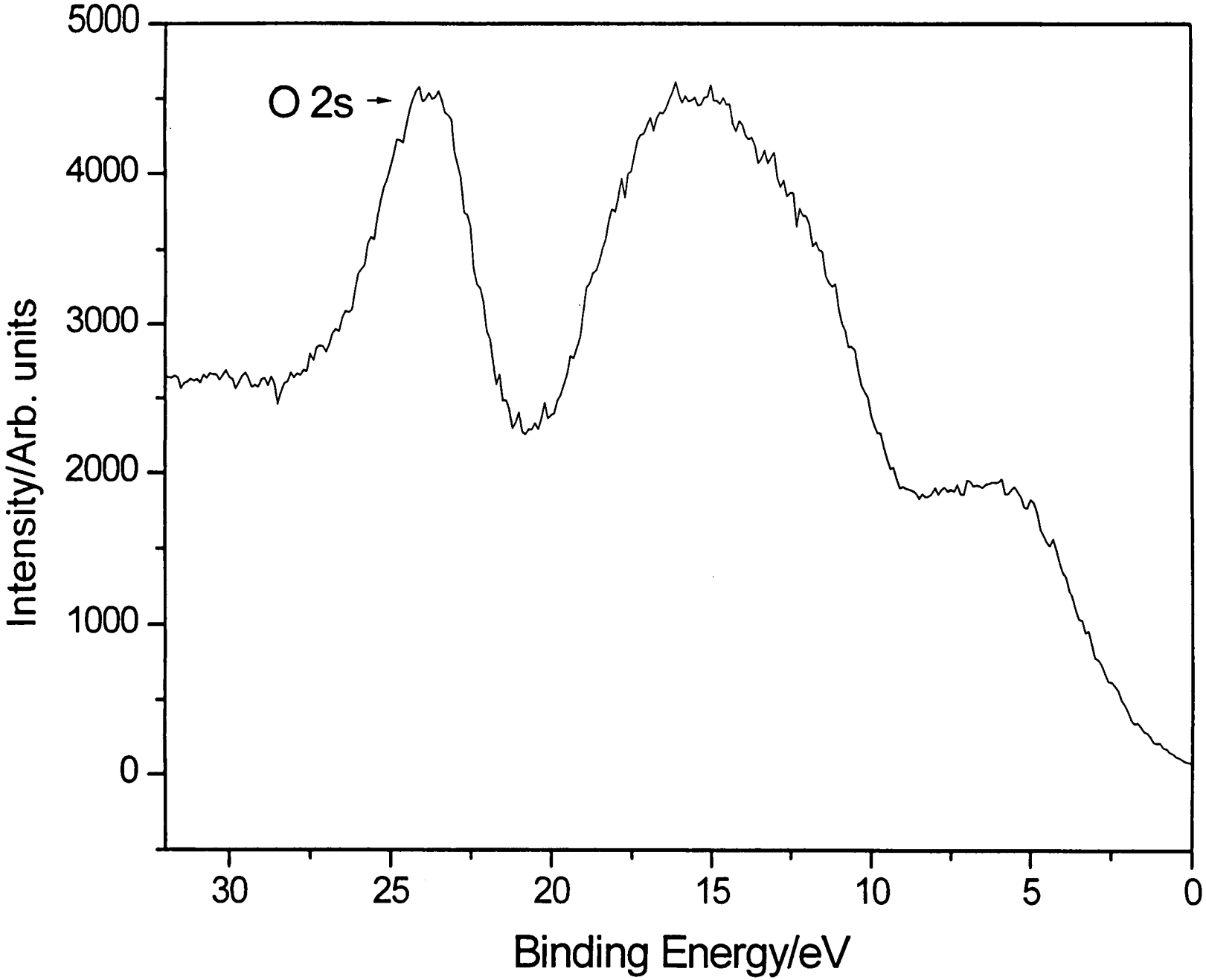
O 2s
5000
4000
3000
2000
1000
0
Intensity/Arb. units
30
25
20
15
10
5
0
Binding Energy/eV

Fig. 9

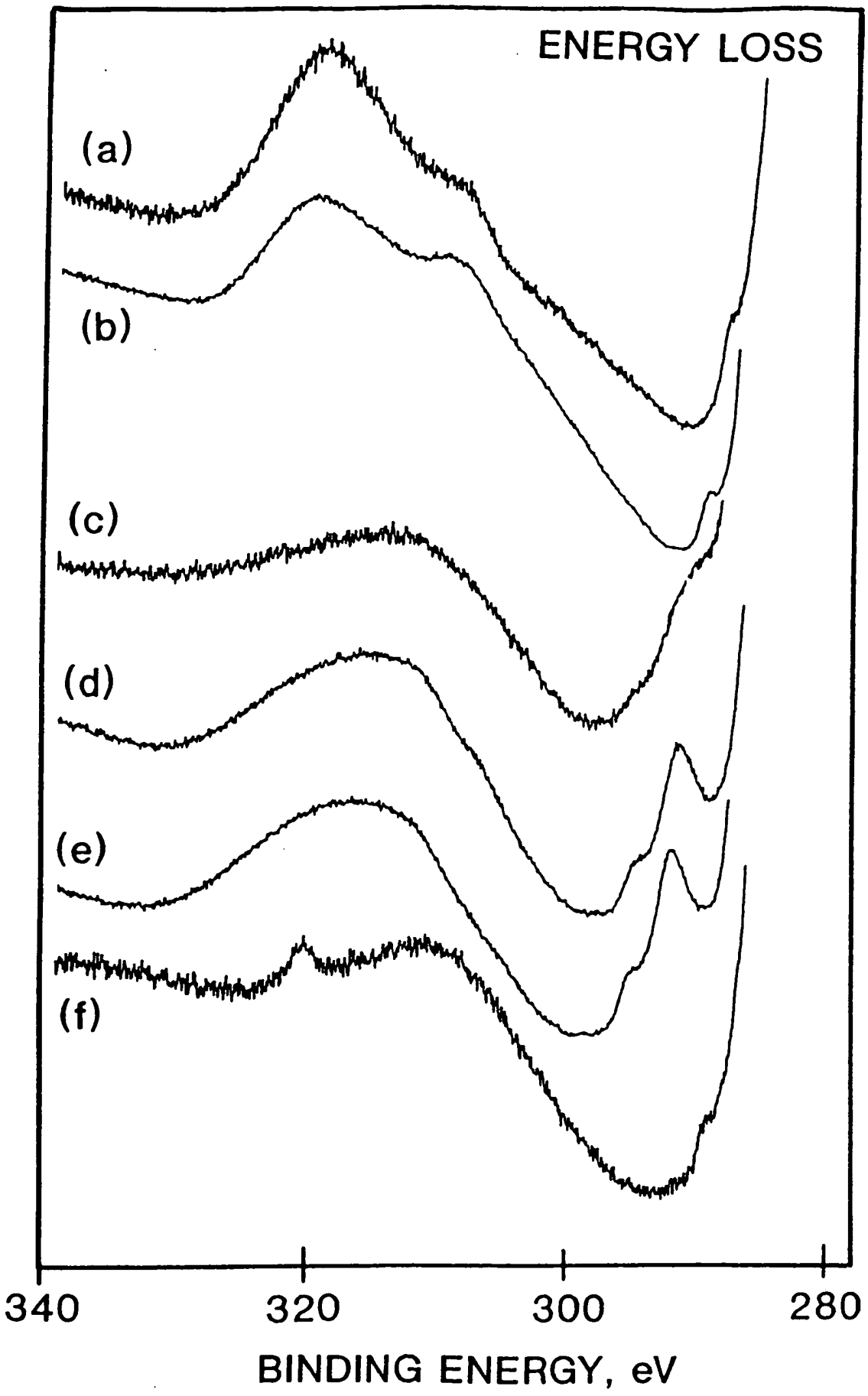

Fig. 10

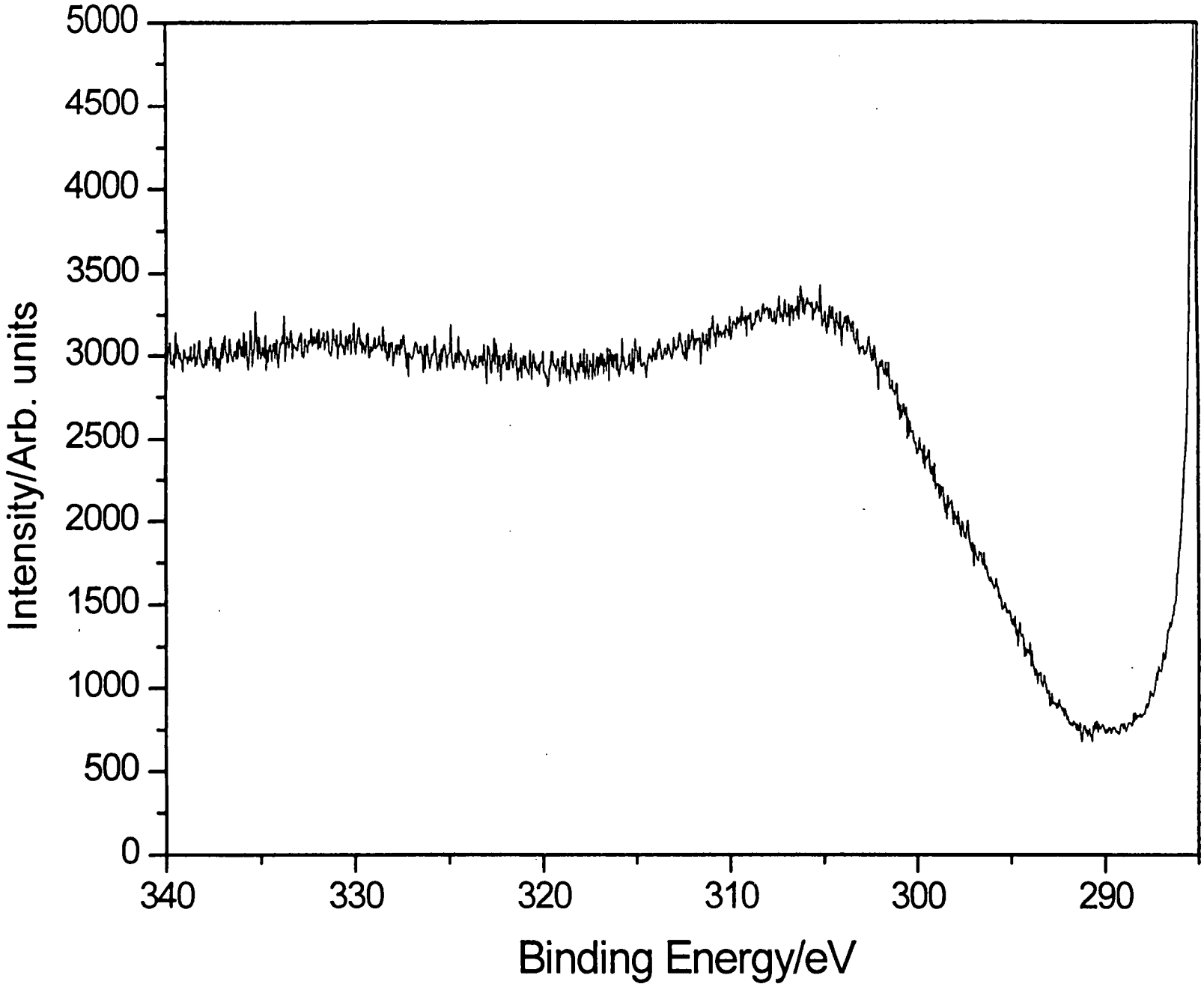
sample: 021802JS
5000
4500
4000
3500
3000
2500
2000
1500
1000
500
0
Intensity/Arb. units
340
330
320
310
300
290
Binding Energy/eV

Fig. 11

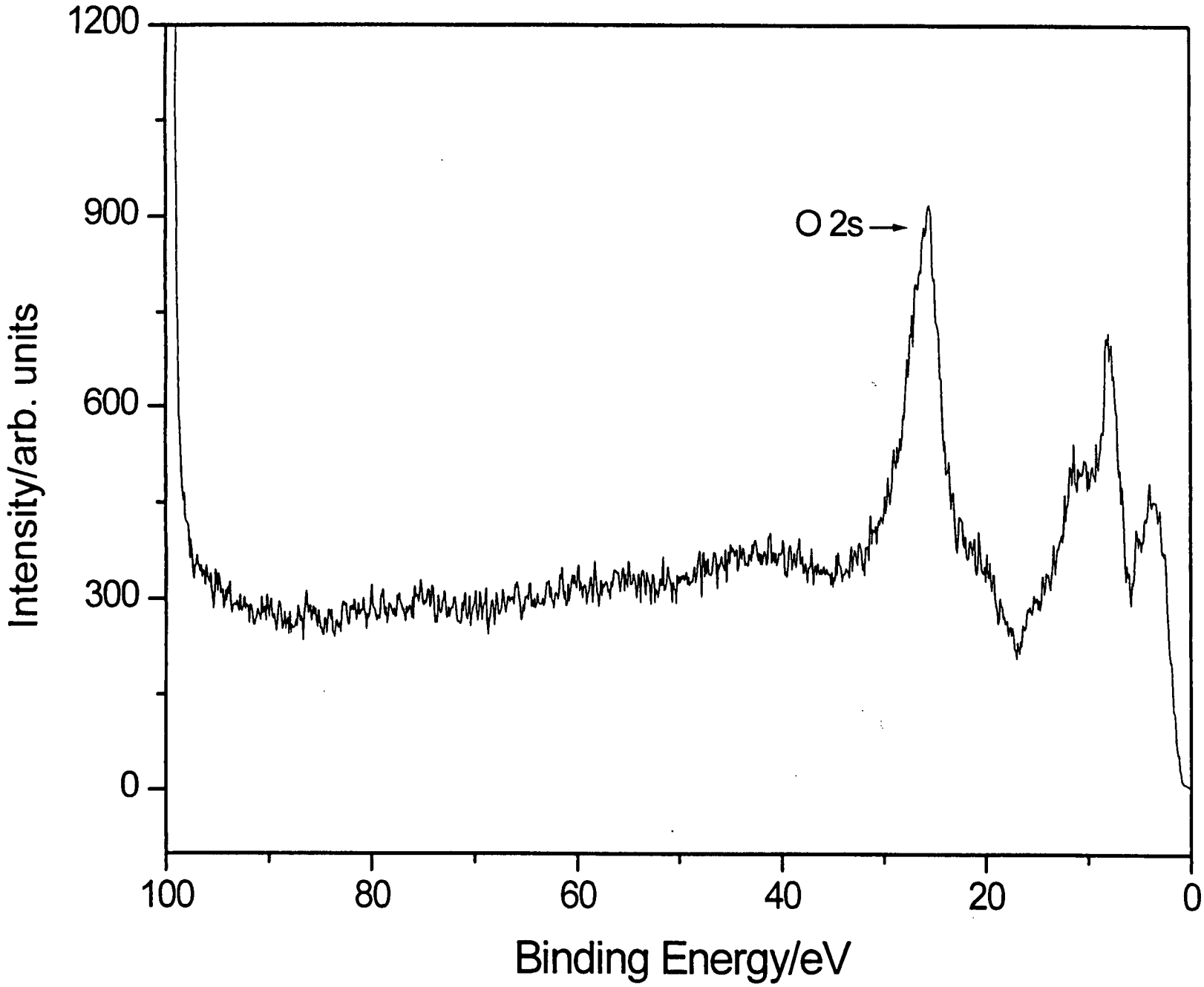
1200
900
600
300
0
Intensity/arb. units
O 2s
100
80
60
40
20
0
Binding Energy/eV

Fig. 12

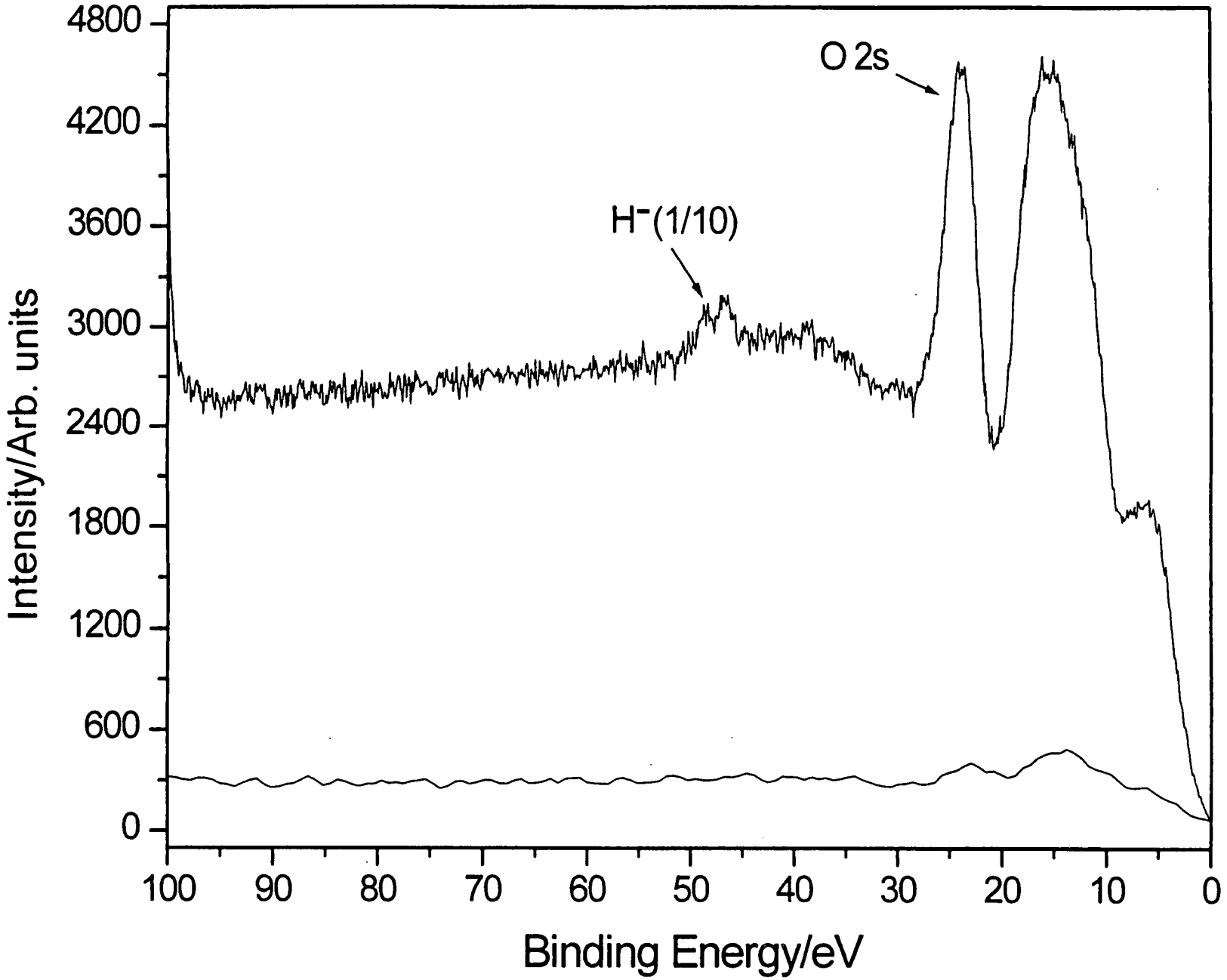
4800
4200
3600
3000
2400
1800
1200
600
0
Intensity/Arb. units
O 2s
H⁻(1/10)
100
90
80
70
60
50
40
30
20
10
0
Binding Energy/eV

Fig. 13

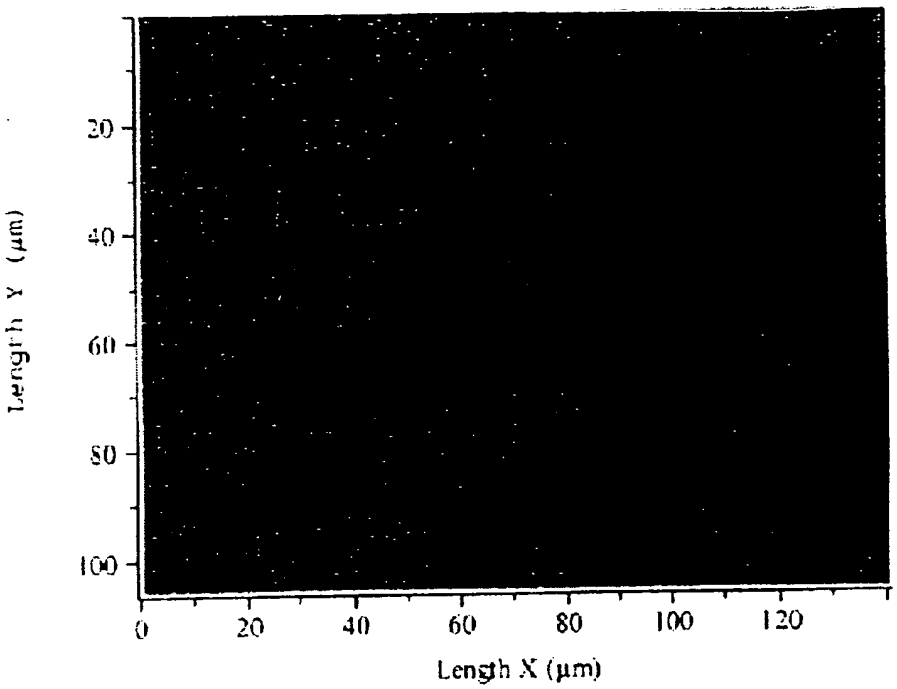

Fig. 14

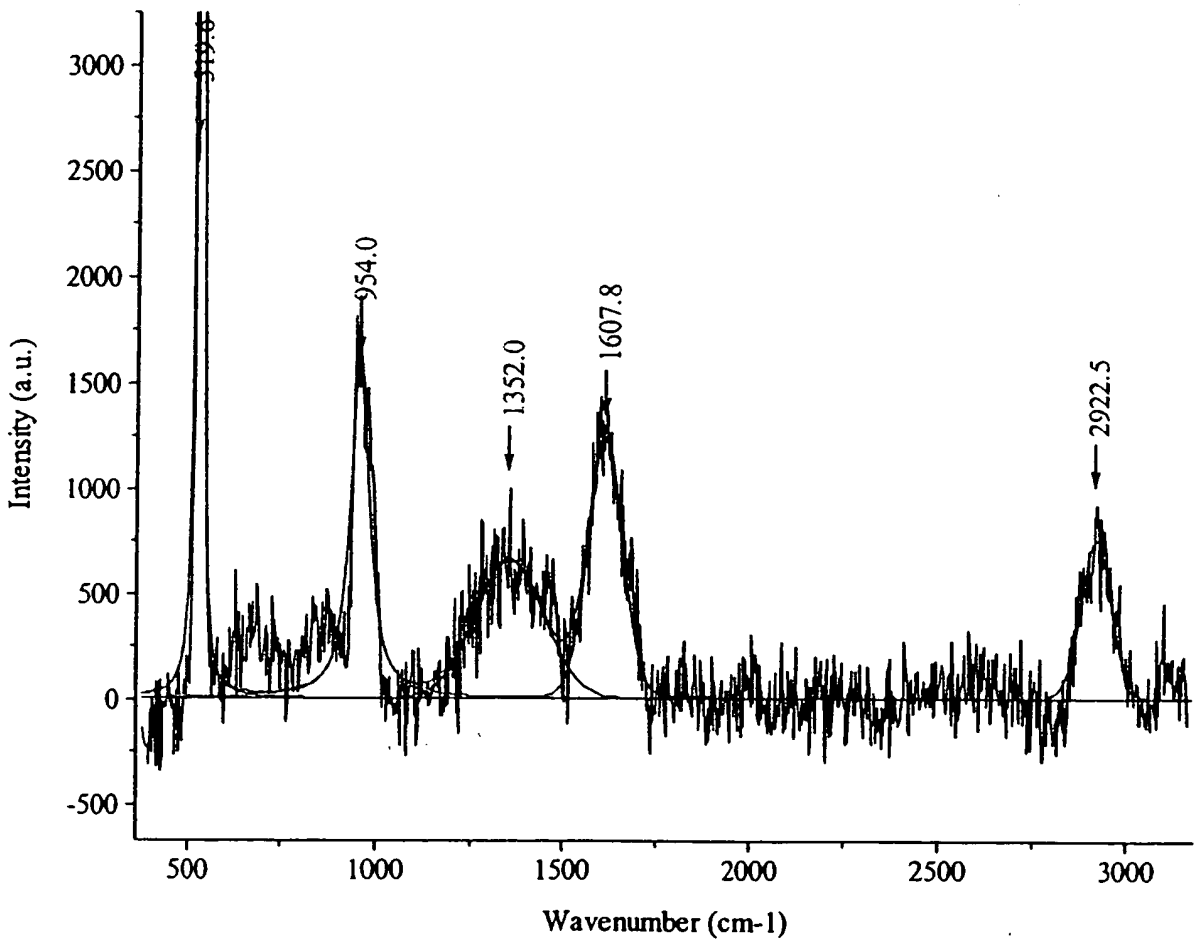
Intensity (a.u.)
3000
2500
2000
1500
1000
500
0
-500
954.0
1352.0
1607.8
2922.5
500
1000
1500
2000
2500
3000
Wavenumber (cm-1)

Fig. 15